

Crystal growth, spectral properties and Judd-Ofelt analysis of Pr: CaF_2-YF_3

Jie Tian(田杰), Xiao Cao(曹笑), Wudi Wang(王无敌), Jian Liu(刘坚), Jianshu Dong(董建树), Donghua Hu(胡冬华), Qingguo Wang(王庆国), Yanyan Xue(薛艳艳), Xiaodong Xu(徐晓东), and Jun Xu(徐军)

Citation: Chin. Phys. B, 2021, 30 (**10**): 108101. DOI: 10.1088/1674-1056/abf921
Journal homepage: http://cpb.iphy.ac.cn; http://iopscience.iop.org/cpb

What follows is a list of articles you may be interested in

Crystal growth, structure and optical properties of Pr^{3+}-doped yttria-stabilized zirconia single crystals

Dai-Ni Wang(王黛妮), Shou-Lei Xu(徐守磊), Xiang-Yu Wang(王翔宇), Si-Yao Li(李思瑶), Xing Hong(洪杏), Bernard A. Goodman, and Wen Deng(邓文)

Chin. Phys. B, 2021, 30 (**7**): 078103. DOI: 10.1088/1674-1056/abfb55

Effects of $MgSiO_3$ on the crystal growth and characteristics of type-Ib gem quality diamond in Fe-Ni-C system

Zhi-Yun Lu(鲁智云), Yong-Kui Wang(王永奎), Shuai Fang(房帅), Zheng-Hao Cai(蔡正浩), Zhan-Dong Zhao(赵占东), Chun-Xiao Wang(王春晓), Hong-An Ma(马红安), Liang-Chao Chen(陈良超), and Xiao-Peng Jia(贾晓鹏)

Chin. Phys. B, 2020, 29 (**12**): 128103. DOI: 10.1088/1674-1056/abb800

Regulation mechanism of catalyst structure on diamond crystal morphology under HPHT process

Ya-Dong Li(李亚东), Yong-Shan Cheng(程永珊), Meng-Jie Su(宿梦洁), Qi-Fu Ran(冉启甫), Chun-Xiao Wang(王春晓), Hong-An Ma(马红安), Chao Fang(房超), Liang-Chao Chen(陈良超)

Chin. Phys. B, 2020, 29 (**7**): 078101. DOI: 10.1088/1674-1056/ab90e8

A low-dimensional crystal growth model on an isotropic and quasi-free sustained substrate

Chenxi Lu(卢晨曦), Senjiang Yu(余森江), Lingwei Li(李领伟), Bo Yang(杨波), Xiangming Tao(陶向明), Gaoxiang Ye(叶高翔)

Chin. Phys. B, 2020, 29 (**3**): 038101. DOI: 10.1088/1674-1056/ab6968

A numerical study on pattern selection in crystal growth by using anisotropic lattice Boltzmann-phase field method

Zhaodong Zhang(张兆栋), Yuting Cao(曹宇婷), Dongke Sun(孙东科), Hui Xing(邢辉), Jincheng Wang(王锦程), Zhonghua Ni(倪中华)

Chin. Phys. B, 2020, 29 (**2**): 028103. DOI: 10.1088/1674-1056/ab6718

Crystal growth, spectral properties and Judd–Ofelt analysis of Pr: CaF_2-YF_3*

Jie Tian(田杰)[1], Xiao Cao(曹笑)[1], Wudi Wang(王无敌)[1], Jian Liu(刘坚)[1], Jianshu Dong(董建树)[1], Donghua Hu(胡冬华)[1], Qingguo Wang(王庆国)[1,†], Yanyan Xue(薛艳艳)[1,‡], Xiaodong Xu(徐晓东)[2], and Jun Xu(徐军)[1]

[1] *School of Physics Science and Engineering, Institute for Advanced Study, Tongji University, Shanghai* 200092, *China*
[2] *Jiangsu Key Laboratory of Advanced Laser Materials and Devices, School of Physics and Electronic Engineering, Jiangsu Normal University, Xuzhou* 221116, *China*

(Received 29 December 2020; revised manuscript received 9 April 2021; accepted manuscript online 19 April 2021)

The 0.6 at.% Pr^{3+}-doped CaF_2-YF_3 crystal was successfully grown by the temperature gradient technique (TGT). X-ray diffraction analysis showed that the grown crystal still had cubic structure. The absorption spectrum, emission spectrum, Judd–Ofelt analysis and fluorescence decay curve at room temperature were discussed. The fluorescence lifetime of Pr: CaF_2-YF_3 crystal was 45.46 μs, and the $\sigma_{em} \cdot \tau$ of $^3P_0 \rightarrow {}^3H_6$ and $^3P_0 \rightarrow {}^3F_2$ transitions were calculated to be 80.92×10^{-20} cm$^2 \cdot$ μs and 388.7×10^{-20} cm$^2 \cdot$ μs, respectively. The FWHMs are 20.1 nm and 6.8 nm, which are higher than those of Pr: $LiYF_4$, Pr: $LiLuF_4$, Pr: $LiGdF_4$ and Pr: BaY_2F_8 crystals. The results show that the Pr: CaF_2-YF_3 crystal is expected to achieve 605 nm orange light and 642 nm red light laser operation.

Keywords: CaF_2-YF_3, crystal growth, spectral property, Judd–Ofelt theory

PACS: 81.10.–h, 42.70.Hj, 02.70.Hm, 61.50.–f **DOI:** 10.1088/1674-1056/abf921

1. Introduction

Inorganic glass has aroused permanent research interest due to its special physical properties. The emission band width of rare-earth ions doped in glass is usually much larger than that of crystals.[1–3] Along with glass, mixed fluoride crystals also have great structural disorder and broad spectral characteristics.[4–6] In highly disordered mixed fluoride crystals, the uneven spectral broadening is very large. Since the emission spectrum is greatly widened, the pump efficiency of the broadband pump source can be improved and the peak stimulated radiation cross section can be reduced.[7] Therefore, highly disordered mixed crystals can be used as a link between glass and ordinary crystals, and have attracted attention due to their unique combination of optical and thermo-mechanical properties.

In the trivalent rare earth ion doped CaF_2 crystal system, when a trivalent ion replaces a divalent Ca^{2+}, an interstitial F^- is required to be introduced into the lattice as a charge compensation. However, even in the case of low doping concentration, the CaF_2 single crystal of this structure is easy to form clusters, which are usually used as emission quenching centers. Therefore, a mixed crystal of CaF_2-ReF_3 (Re = Y, La, Gd, Lu) is proposed to replace the usual CaF_2 single crystal.[8] When x is greater than 0.1, the $(CaF_2)_{1-x}$-$(YF_3)_x$ system exhibits the broad emission spectrum characteristics of glass.[9] The degree of disorder of the structure is mainly controlled by the variation of the Y^{3+} concentration.[10]

Pr^{3+} has a large number of emission transitions in the visible light band and efficient laser emissions in the blue, green, orange, red and deep red spectral regions have been obtained in Pr^{3+}-doped laser materials.[11–18] By incorporating the modifier ion Gd^{3+}, a 642 nm red laser is obtained in the Pr: CaF_2 crystal with an output power of 22.2 mW.[19] However, crystal growth and spectral properties of Pr^{3+}-doped CaF_2-YF_3 crystal have not been investigated. In this paper, the Pr: CaF_2-YF_3 single crystal has been successfully grown by the temperature gradient technique (TGT). The structure, spectral properties and Judd–Ofelt (J-O) analysis of Pr: CaF_2-YF_3 crystal were studied.

2. Crystal growth

The high-quality 0.6 at.% Pr^{3+}-doped CaF_2-YF_3 crystal was grown by the TGT as shown in Fig. 1. The starting materials were Pr_6O_{11} [4N], CaF_2 [4N] and YF_3 [4N] weighed out according to the molecular formula $Pr_{0.006}Y_{0.285}Ca_{0.709}F_2$, and 1 at.% PbF_2 was used as an oxygen scavenger mixed in CaF_2 powder. The powder was mixed in an agate pot and loaded into a graphite crucible. The graphite crucible was sealed in a high-purity argon environment to prevent oxidation. The temperature rise rate was 300–400 °C/h to 1430 °C, and the temperature was kept constant for 3–4 h until the raw material was completely melted in the first stage. The

*Project supported by the National Natural Science Foundation of China (Grant Nos. 61805177, 61861136007, and 61621001).
†Corresponding author. E-mail: qgwang@tongji.edu.cn
‡Corresponding author. E-mail: xueyanyanf@163.com
© 2021 Chinese Physical Society and IOP Publishing Ltd

temperature drop rate was 0.5–1.5 °C/h at the equal diameter stage for 120 h, and after the growth the crystals were cooled to the room temperature at the relatively fast rate. The grown Pr: CaF_2-YF_3 crystal was transparent with the size of $\Phi 15 \times 45$ mm^3, which is shown in Fig. 1(a). The $\Phi 15 \times 2$ mm^3 crystal sample was cut from the middle part of the Pr: CaF_2-YF_3 crystal, and two surfaces were polished to $\Phi 15 \times 1.5$ mm^3 for spectra measurement, which is shown in Fig. 1(b).

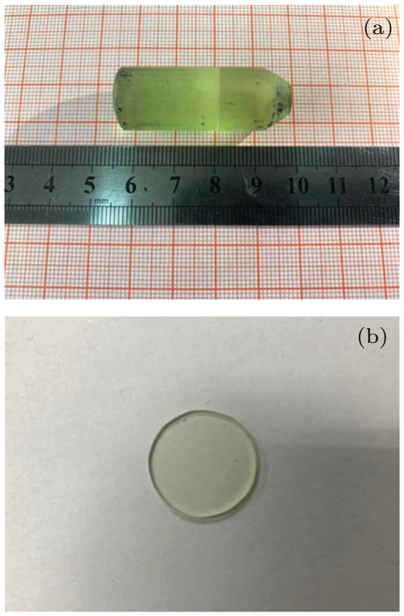


Fig. 1. (a) The photo of the grown Pr: CaF_2-YF_3 crystal. (b) The polished sample of the Pr: CaF_2-YF_3 crystal.

The sample was cut from the crystal in the middle position and ground into powder for x-ray powder diffraction (XRD) and inductively coupled plasma atomic emission spectroscopy (ICP-AES) measurement. The structure of the sample was analyzed by an automated Ultima IV diffractometer (Rigaku, Japan). The XRD pattern of the Pr: CaF_2-YF_3 crystal is shown in Fig. 2(a), which is consistent with the JCPDS card (PDF# 31-0923), and there is no extra impurity peak, indicating that Pr: CaF_2-YF_3 still belongs to the cubic crystal system. The calculated Pr: CaF_2-YF_3 crystal unit cell parameter is 5.4901 Å. At the same time, the XRD of 0.6 at.% Pr: CaF_2 is shown in Fig. 2(b), which is consistent with the JCPDS card (PDF# 35-0816). The calculated Pr: CaF_2 crystal unit cell parameter is 5.4631 Å. With the doping of Y^{3+} ions, the crystal unit cell parameters become larger. This is due to the fact that Y^{3+} ions enter substitutional for Ca^{2+} ions into the melt, resulting in interstitial F^- ions for charge compensation, and the interstitial F^- ion radius is 1.33 Å, which makes the crystal lattice expansion. The concentrations of Pr^{3+} ions and Y^{3+} ions in the middle of the Pr: CaF_2-YF_3 crystal were 0.63 at.% and 25.49 at.%, respectively, which was measured by inductively coupled plasma atomic emission spectrometry (ICP-AES).

The absorption spectra from 400–2500 nm were measured by a UV-VIS-NIR spectrophotometer (Lambda900, Perkin-Elmer) at room temperature. The room temperature fluorescence spectra in the wavelength range of 450–800 nm and the fluorescence lifetime at 481 nm were recorded by Edinburgh Instruments FLS980 spectrophotometer under 443 nm excitation.

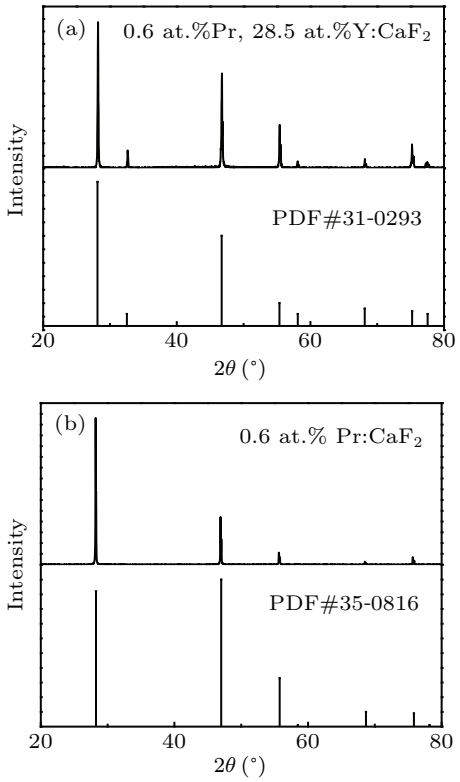


Fig. 2. (a) XRD pattern of Pr: CaF_2-YF_3 crystal and standard pattern of CaF_2-YF_3, (b) XRD pattern of Pr: CaF_2 crystal and standard pattern of CaF_2.

3. Results and discussion

Figure 3 shows the absorption spectra of the Pr: CaF_2-YF_3 crystal from 400 nm to 2500 nm at room temperature. The absorption spectra are mainly composed of eight absorption bands, corresponding to the $^3H_4 \rightarrow {}^3P_2$, $^3P_1+{}^1I_6$, $^3P_0$, $^1D_2$, $^1G_4$, $^3F_3+{}^3F_4$, $^3F_2$, and $^3H_6$ transitions, respectively. The absorption peak wavelength at 443 nm corresponds to the $^3H_4 \rightarrow {}^3P_2$, the absorption coefficient is 1.44 cm^{-1}, and the FWHM is 17.8 nm. The absorption cross section at 443 nm is calculated to be 0.77×10^{-20} cm^2, which shows that the Pr: CaF_2-YF_3 crystal is easy to perform laser operation under GaN/InGaN LD pumping.

In 1962, Judd and Ofelt proposed the Judd–Ofelt (J-O) theory, and used it to reasonably explain the energy level transition of rare earth ions, which became a common method for analyzing the spectral properties of rare earth ions in glass and crystal materials.[20,21] Generally speaking, the absorption band is mainly caused by the electric-dipole transition, so this formula does not consider the magnetic dipole transition.[22,23]

The experimental line strength $S_{\rm exp}(J\to J')$ of the electric-dipole transition can be defined by the following formula:

$$S_{\rm ep}(J,J') = \frac{3hc(2J+1)}{8\pi^3e^2N}\frac{9n}{(n^2+1)^2}\frac{\ln 10}{L\overline{\lambda}} \times \int {\rm OD}(\lambda)\,{\rm d}\lambda, \quad (1)$$

where h is the Planck constant, c is the speed of light in vacuum, e is the electron charge, N is the concentration of Pr^{3+} ion doping, n represents the refractive index of the CaF_2-YF_3 crystal, λ is the average wavelength of the absorption band corresponding to the $J\to J'$ transition, L is the thickness of the Pr:CaF_2-YF_3 sample, and OD(λ) represents the measured optical density. According to the J-O theory, the strength of the line $S_{\rm cal}(J,J')$ can be calculated by the following formula:

$$S_{\rm cal}(J,J') = \sum_{t=2,4,6}\Omega_t|\langle(S,L)J||U^{(t)}||(S',L')J'\rangle|^2, \quad (2)$$

where J and J' are the angular momentum quantum numbers of the initial and final energy levels, $\langle||U^{(t)}||\rangle$ represents the squared matrix elements, Ω_t ($t=2,\ 4,\ 6$) is the J-O intensity parameter. According to the absorption spectra, the calculated average wavelength, experimental absorption line intensity $S_{\rm exp}(J,J')$ and theoretical line intensity $S_{\rm cal}(J,J')$ are shown in Table 1.

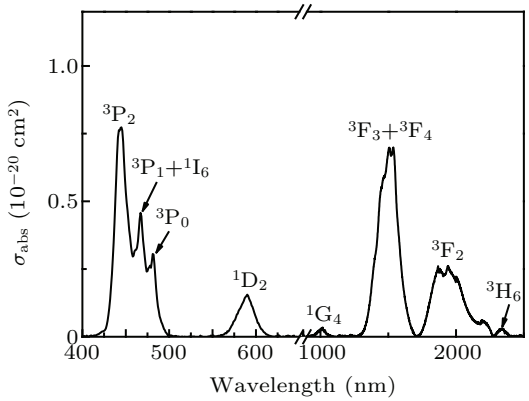


Fig. 3. Absorption spectra of Pr^{3+}-doped CaF_2-YF_3 crystal at room temperature.

Table 1. The calculated average wavelength λ, refractive index n, absorption line strength $S_{\rm exp}(J,J')$ and calculated line strength $S_{\rm cal}$ (J,J') of the Pr: CaF_2-YF_3 crystal.

Transition (from $^3H_4$)	λ (nm)	$S_{\rm exp}$ (10^{-20} cm^2)	$S_{\rm cal}$ (10^{-20} cm^2)
$^3P_2$	443	1.397	0.660
$^3P_1$+$^1I_6$	467	0.127	0.135
$^3P_0$	482	0.064	0.003
$^1D_2$	589	0.326	0.257
$^1G_4$	1002	0.092	0.131
$^3F_3$+$^3F_4$	1498	5.921	5.892
$^3F_2$	1918	1.402	1.370
$^3H_6$	2349	0.044	0.679
RMSΔS (10^{-20} cm^2)		0.438	

The root-mean-square deviation between the experiment and calculation line strengths can be obtained by the following equation:

$${\rm RMS\Delta S} = \sqrt{\sum_{J'}(S_{\rm exp}-S_{\rm cal})^2/(N-3)}, \quad (3)$$

where N is the number of absorption bands used in the calculation. The RMSΔS is 0.438×10^{-20} cm^2, which shows that the measured spectral intensity is in good agreement with the calculated spectral intensity. Through the least square fitting of $S_{\rm exp}(J,J')$ and $S_{\rm cal}(J,J')$, the J-O intensity parameters can be obtained. According to this formula, the Ω_2, Ω_4, and Ω_6 of the CaF_2-YF_3 crystal were calculated as 1.55×10^{-20} cm^2, 0.02×10^{-20} cm^2, and 4.86×10^{-20} cm^2, respectively. The J-O intensity parameters of Pr^{3+} in CaF_2-YF_3 and other crystals are listed in Table 2.

Table 2. The J-O intensity parameters of Pr^{3+} in CaF_2-YF_3 and other crystals.

Crystals	Ω_2 (10^{-20} cm^2)	Ω_4 (10^{-20} cm^2)	Ω_6 (10^{-20} cm^2)	Ref.
$CaYAlO_4$	5.67	8.09	14.90	[16]
$LiYF_4$	3.45	3.94	6.13	[18]
CaF_2	1.15	3.6	10	[18]
KYF_4	3.92	1.78	7.94	[18]
BaY_2F_8	1.09	3.49	2.22	[18]
LaF_3	0.72	0.39	4.79	[24]
$YAlO_3$	2.28	3.88	5.15	[25]
$Y_3Al_5O_{12}$	0	12.20	8.17	[26]
CaF_2-YF_3	1.55	0.02	4.86	this work

The value of Ω_2 represents the covalency of the doped ions and the anion in the ligand, which reflects the symmetry of the crystal field. The value of Ω_2 of Pr: CaF_2-YF_3 is higher than that of Pr^{3+}-doped LaF_2, CaF_2, BaY_2F_8 , which indicates that the covalency of Pr^{3+} ions in CaF_2-YF_3 is higher than that in LaF_2, CaF_2 and BaY_2F_8. The Ω_4 and Ω_6 are related to the crystal structure and usually important parameters to describe the spectral quality. The value of Ω_4/Ω_6 of Pr: CaF_2-YF_3 is 0.004, which is smaller than that of Pr^{3+}-doped LaF_2, $LiYF_4$, CaF_2, and BaY_2F_8. The results show that the rigidity of Pr: CaF_2-YF_3 is smaller than that of Pr^{3+}-doped LaF_2, $LiYF_4$, CaF_2, and BaY_2F_8.

The radiative transition rates $A(J\to J')$ from the excited state $^3P_0$ to other lower state are calculated by the following equation:

$$\begin{aligned} &A\left[(S,L)J;(S',L')J'\right] \\ &= A_{\rm ed}+A_{\rm md} \\ &= \frac{64\pi^4e^2}{3h(2J+1)\overline{\lambda}^3}\left[\frac{n(n^2+2)^2}{9}S_{\rm ed}+n^3S_{\rm md}\right], \end{aligned} \quad (4)$$

where $A_{\rm ed}$ is the probability of electric dipole radiation transition, $A_{\rm md}$ is the probability of magnetic dipole radiation transition, $A_{\rm ed}$ is the electric dipole radiation transition probability, $A_{\rm md}$ is the magnetic dipole radiation transition probability, $S_{\rm ed}$ is the electric dipole radiation intensity, and $S_{\rm md}$ is the magnetic dipole radiation intensity. Among them, $S_{\rm md}$ is a constant

that is not related to the material, and S_{ed} is determined by the following formula:

$$S_{ed} = \Omega_2 \cdot U_2 + \Omega_4 \cdot U_4 + \Omega_6 \cdot U_6. \tag{5}$$

The fluorescence branch ratio of each spectral line is defined as

$$\beta(J \to J') = \frac{A(J \to J')}{\sum_{J'} A(J \to J')}. \tag{6}$$

The radiation lifetime is calculated by the following formula:

$$\tau_{rad} = \frac{1}{\sum_{J'} A(J \to J')}. \tag{7}$$

The spontaneous transition rate, branch ratio and radiation lifetime of the $^3P_0$ energy level in Pr: CaF_2-YF_3 crystal are listed in Table 3. The radiation lifetime was calculated to be 158.4 μs, which is longer than that of Pr: CYA (9.7 μs),[15] Pr: LaF_2 (88.36 μs),[24] Pr: YAP (19.99 μs),[25] Pr: $KLu(WO_4)_2$ (10.18 μs)[27] and Pr: $SrWO_4$ (9.5 μs)[28] crystals. The results show that the Pr: CaF_2-YF_3 crystal has high energy storage capacity and easy for laser operation.

Table 3. Radiative transition rates $A(J,J')$, branching ratios $\beta(J,J')$ and radiative lifetime τ_{rad} of Pr: CaF_2-YF_3 crystal.

Transitions (from $^3P_0$)	$\bar{\lambda}$ (nm)	A_{ed} (s^{-1})	β (%)
$^3H_4$	485	55.91	0.89
$^3H_5$	531	0	0
$^3H_6$	607	2995.44	47.46
$^3F_2$	644	3250.3	51.49
$^3F_3$	699	0	0
$^3F_4$	724	10.47	0.16
Radiative lifetime	158.4 μs		

The fluorescence spectra of the Pr: CaF_2-YF_3 crystal in the range of 450–800 nm under excitation of 443 nm is shown in Fig. 4. The simplified energy level diagram for the Pr: CaF_2-YF_3 crystal is shown in Fig. 5. There are seven emission bands, which correspond to $^3P_0 \to {}^3H_4$ (around 481 nm), $^3P_{0,1} \to {}^3H_5$ (around 525 nm), $^3P_0 \to {}^3H_6$ (around 606 nm), $^3P_0 \to {}^3F_2$ (around 642 nm), $^3P_0 \to {}^3F_3$ (around 699 nm) and $^3P_0 \to {}^3F_4$ (around 725 nm).

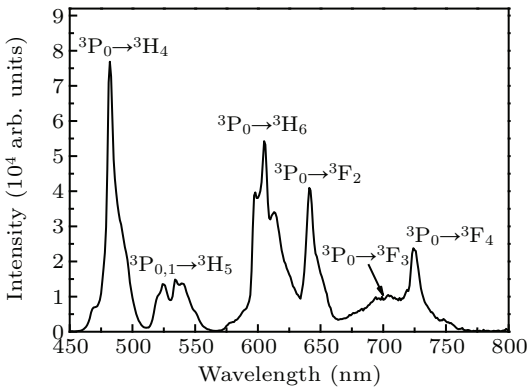


Fig. 4. Room temperature fluorescence spectra of Pr: CaF_2-YF_3 crystal in visible region under excitation at 443 nm.

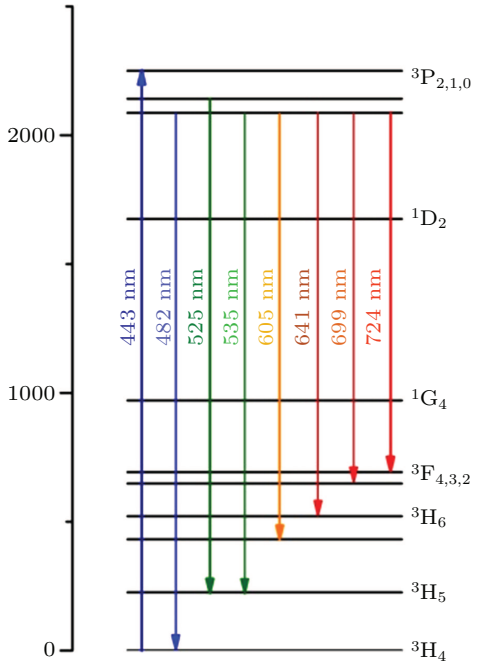


Fig. 5. Simplified energy level diagram level in Pr: CaF_2-YF_3 crystal.

The stimulated radiation cross section is one of the important parameters for the performance of laser, which is calculated by the F-L formula[29]

$$\sigma_{em}(\lambda)_{JJ'} = \frac{A(J,J')\lambda^5}{8\pi n^2 c} \frac{I(\lambda)}{\int_{band} \lambda I(\lambda) d\lambda}, \tag{8}$$

where $A(J,J')$ is the radiative transition rates, $I(\lambda)$ is the experimental fluorescent intensity at the wavelength λ, n is the refractive index, and c stands for the light velocity. The parameters of emission cross section σ_{em}, FWHM and peak wavelength λ are calculated and listed in Table 4.

Table 4. The emission cross section σ_{em}, FWHM and peak wavelength λ.

Transitions	Peak wavelength (nm)	FWHM (nm)	σ_{em} (10^{-20} cm^2)
$^3P_0 \to {}^3H_4$	481	10.6	0.18
$^3P_0 \to {}^3H_6$	605	20.1	1.78
$^3P_0 \to {}^3F_2$	641	6.8	4.61
$^3P_0 \to {}^3F_4$	724	5.9	0.7

Among them, the red-light emission cross section is the largest at 641 nm, reaching 4.61×10^{-20} cm^2 and FWHM is 6.8 nm, which corresponds to the $^3P_0 \to {}^3F_2$ transition. In addition, the emission cross section at 605 nm is 1.78×10^{-20} cm^2 and FWHM is 20.1 nm, which corresponds to the $^3P_0 \to {}^3H_6$ transition. The emission cross section is smaller than that of Pr: $LiYF_4$,[30] Pr: $LiLuF_4$,[30] Pr: $LiGdF_4$[30] and Pr: BaY_2F_8,[31] but the FWHMs of the two emission lines are much larger than those of Pr: $LiYF_4$, Pr: $LiLuF_4$, Pr: $LiGdF_4$ and Pr: BaY_2F_8, showing the broad-spectrum characteristics similar to glass. Obviously, the probable radiation transitions are mainly the transitions of $^3P_0 \to {}^3H_6$ and $^3P_0 \to {}^3F_2$, which have probabilities of 47.46% and 51.49%, respectively. The

results show that in the Pr: CaF_2-YF_3 crystal, it is expected to achieve 605 nm orange light and 642 nm red light laser operation.

The room-temperature fluorescence decay curve of the Pr: CaF_2-YF_3 crystal at 481 nm under 443 nm exciting is shown in Fig. 6. The measured decay curve shows a single exponential decay, and the fitted fluorescence lifetime is 45.46 μs, which is longer than that of Pr: $LiYF_4$ (35.7 μs),[30] Pr: $LiLuF_4$ (37.9 μs),[30] Pr: $LiGdF_4$ (43.6 μs)[30] and Pr: BaY_2F_8 (43 μs).[31] The longer fluorescence lifetime indicates that the Pr: CaF_2-YF_3 crystal has a large number of upper-level particles, which is easy for laser operation. The laser quality factor is characterized by $\sigma_{em}\tau$, and the larger value of $\sigma_{em}\tau$ is better for laser operation. The wavelength λ, emission cross-section σ_{em} and $\sigma_{em}\tau$ for the $^3P_0 \rightarrow {}^3H_6$ and $^3P_0 \rightarrow {}^3F_2$ transitions of the Pr^{3+}-doped CaF_2-YF_3 and other crystals are listed in Table 5.

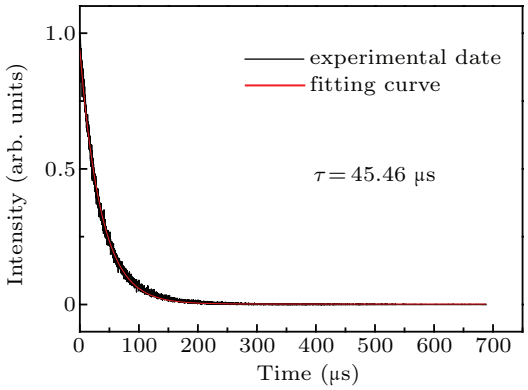


Fig. 6. Room temperature fluorescence decay curve of Pr: CaF_2-YF_3 crystal at 481 nm under excitation at 443 nm.

Table 5. The wavelength λ, emission cross-section σ_{em} and $\sigma_{em}\tau$ for the $^3P_0 \rightarrow {}^3H_6$ and $^3P_0 \rightarrow {}^3F_2$ transitions of Pr^{3+}-doped CaF_2-YF_3 and other crystals that have achieved laser operation.

Crystal	Transitions	Wavelength (nm)	FWHM (nm)	τ_f (μs)	σ_{em} (10^{-20} cm^2)	$\sigma_{em}\tau$ (10^{-20} cm$^2\cdot$μs)	Ref.
Pr: $LiYF_4$	$^3P_0 \rightarrow {}^3H_6$	607	1,4	35.7	14	499.8	[30]
Pr: $LiLuF_4$		607	1.2	37.9	12	454.8	[30]
Pr: $LiGdF_4$		607	1.3	43.6	13	566.8	[30]
Pr: BaY_2F_8		607	1.2	43	24.7	1062.1	[31]
Pr: CaF_2-YF_3		605	20.1	45.46	1.78	80.92	this work
Pr: $LiYF_4$	$^3P_0 \rightarrow {}^3F_2$	640	2.2	35.7	22	784.5	[30]
Pr: $LiLuF_4$		640	2.1	37.9	21	795.9	[30]
Pr: $LiGdF_4$		640	2.3	43.6	23	1003	[30]
Pr: BaY_2F_8		639	0.6	43	12.1	388.7	[31]
Pr: CaF_2-YF_3		641	6.8	45.56	4.61	209.57	this work

The $\sigma_{em}\tau$ of $^3P_0 \rightarrow {}^3H_6$ and $^3P_0 \rightarrow {}^3F_2$ transitions are found to be 80.92×10^{-20} cm$^2\cdot$μs and 388.7×10^{-20} cm$^2\cdot$μs, respectively, which are smaller than those of Pr: $LiYF_4$, Pr: $LiLuF_4$, Pr: $LiGdF_4$ and Pr: BaY_2F_8 crystals. However, the FWHM of Pr^{3+}-doped CaF_2-YF_3 is much larger than that of Pr^{3+}-doped other crystals. Ultrafast laser requires not only a large value of $\sigma_{em}\tau$, but also a large stimulated emission bandwidth. The $\sigma_{em}\tau$ multiplied by FWHM of the Pr^{3+}-doped CaF_2-YF_3 is higher than that of Pr^{3+}-doped other crystals. The above results demonstrate that the $^3P_0 \rightarrow {}^3H_6$ and $^3P_0 \rightarrow {}^3F_2$ transitions of the Pr: CaF_2-YF_3 crystal are promising for orange and red ultrafast laser operation.

4. Conclusion

The 0.6 at.% Pr^{3+}-doped CaF_2-YF_3 crystal was successfully grown by the TGT. The absorption spectrum, emission spectrum, J-O analysis and fluorescence decay curve at room temperature were discussed. The absorption cross-sections at 443 nm were calculated to be 0.77×10^{-20} cm^2 and the values of Ω_2, Ω_4, and Ω_6 were calculated to be 1.55×10^{-20} cm^2, 0.02×10^{-20} cm^2 and 4.86×10^{-20} cm^2, respectively. In addition, the emission cross sections were calculated to be 1.78×10^{-20} cm^2 at 605 nm and 4.61×10^{-20} cm^2 at 642 nm with FWHMs of 20.1 nm and 6.8 nm, respectively, which correspond to the $^3P_0 \rightarrow {}^3H_6$ and $^3P_0 \rightarrow {}^3F_2$ transitions. The fluorescence lifetime of the Pr: CaF_2-YF_3 crystal was 45.46 μs and the $\sigma_{em}\tau$ of $^3P_0 \rightarrow {}^3H_6$ and $^3P_0 \rightarrow {}^3F_2$ transitions were calculated to be 80.92×10^{-20} cm$^2\cdot$μs and 388.7×10^{-20} cm$^2\cdot$μs, respectively, which show that the Pr: CaF_2-YF_3 crystal is promising for orange and red ultrafast laser operation.

References

[1] Weber M J, Myers J D and Blackburn D H 1981 *J. Appl. Phys.* **52** 2944
[2] Avakyants L I, Buzhinskiĭ I M, Koryagina E I and Surkova V F 1978 *Sov. J. Quantum Electron.* **8** 423
[3] Lei G, Anderson J E, Buchwald M I, Edwards B C and Epstein R I 1998 *Phys. Rev. B* **57** 7673
[4] Jang K W and Meltzer R S 1995 *Phys. Rev. B* **52** 6431
[5] BasievA T T, Karasik A Ya and Shubochkin R L 1995 *J. Lumin.* **64** 259
[6] Dianov E M, Karasik A Ya and Shcherbakov I A 1977 *Sov. J. Quantum Electron.* **7** 588
[7] Chase L L, Payne S A and Wilke G D 1987 *J. Phys. C: Solid State Phys.* **20** 953
[8] Wu Y, Su L, Wang Q, Li H, Zhan Y, Jang D, Qian X, Wang C, Zheng L, Chen H, Xu J, Ryba-Romanowski W, Solarz P and Lisiecki R 2013 *Laser Phys.* **23** 105805
[9] FitzGerald S A, Campbell J A and Sievers A J 1996 *J. Non. Cryst Solids* **203** 165
[10] Beck W, Karasik A, Arvanitidis J, Basiev T, Flytzanis C, Chase L L, Payne S A and Wilke G D 2000 *J. Lumin.* **86** 289
[11] Zhu P F, Zhang C M, Zhu K, Ping Y X, Song P, Sun X H, Wang F X and Yao Y 2018 *Opt. Laser Technol.* **100** 75

[12] Gong X H, Xiong F B, Lin Y F, Tan Q G, Luo Z D and Huang Y D 2007 *Mater. Res. Bulletin* **42** 413
[13] Wang Y, Li J F, You Z Y, Zhu Z J and Tu C Y 2010 *J. Alloys Compd.* **502** 184
[14] Cao J F, Wang Y, Ma X H, Li J F, Zhu Z J, You Z Y, Yang F G, Sun C L, Cao T, Ji Y X and Tu C Y 2010 *J. Alloys Compd.* **509** 185
[15] Lv Z S, Wang Y, Zhu Z J, You Z Y, Li J F, Gao S F, Wang H Y and Tu C Y 2014 *Appl. Phys. B* **116** 83
[16] Okamoto H, Kasuga K, Hara I and Kubota Y 2009 *Opt. Express* **17** 20227
[17] Khiari S, Velazquez M, Moncorgé R, Doualan J L, Camy P, Ferrier A and Diaf M 2008 *J. Alloys Compd.* **451** 128
[18] Hashimoto K and Kannari F 2007 *Opt. Lett.* **32** 2493
[19] Yu H, Qian X, Guo L, Jiang D, Wu Q, Tang F, Su L, Ju Q, Wang J and Xu J 2018 *Opt. Mater.* **78** 88
[20] Judd B R 1962 *Phys. Rev.* **127** 750
[21] Ofelt G S 1962 *J. Chem. Phys.* **37** 511
[22] Babu P and Jayasankar C K 2001 *Physica B* **301** 326
[23] W Guo, Y Lin, X Gong, Y Chen, Z Luo and Y Huang 2008 *J. Phys. Chem. Solids.* **69** 8
[24] Li N, Xue Y Y, Li D Z, Xu X D, Wang Q G and Xu J 2019 *Mater. Res. Express* **6** 116209
[25] Liu B, Shi J J, Wang Q G, Tang H L, Liu J F, Zhao H Y, Li D Z, Liu J, Xu X D, Wang Z S and Xu J 2018 *J. Lumin.* **196** 76
[26] Malinowski M, Wolski R and Woliński W 1990 *Solid State Commun.* **74** 17
[27] Yu Y, Zhu X, Zhang X, Yuan J, Yu H, Kuang F, Xiong Z, Liao J, Zhang W and Wang G 2016 *Opt. Rev.* **23** 391
[28] Jia G, Wang H, Lu X, You Z, Li J, Zhu Z and Tu C 2007 *Appl. Phys. B* **90** 497
[29] Aull B and Jenssen H 1982 *IEEE J. Quantum Elect.* **18** 925
[30] Cornacchia F, Lieto Di A, Tonelli M, Richter A, Heumann E and Huber G 2008 *Opt. Express* **16** 15932
[31] Hakim R, Damak K, Toncelli A, Fourati M and Maalej R 2013 *J. Lumin.* **143** 233